1-1-2020

Performance of a dual helical ribbon impeller in a two-phase (gas-liquid) stirred tank reactor

Maryam Amiraftabi
Edith Cowan University, m.amiraftabi@ecu.edu.au

Mehdi Khiadani
Edith Cowan University, m.khiadani@ecu.edu.au

Hussein A. Mohammed
Edith Cowan University, Hussein.mohammed@ecu.edu.au

10.1016/j.cep.2020.107811
Amiraftabi, M., Khiadani, M., & Mohammed, H. A. (2020). Performance of a dual helical ribbon impeller in a two-phase (gas-liquid) Stirred Tank Reactor. *Chemical Engineering and Processing: Process Intensification, 148*, Article 107811.
https://doi.org/10.1016/j.cep.2020.107811

Chemical Engineering & Processing: Process Intensification 148 (2020) 107811

Contents lists available at ScienceDirect

Chemical Engineering & Processing: Process Intensification

journal homepage: www.elsevier.com/locate/cep

Performance of a dual helical ribbon impeller in a two-phase (gas-liquid) stirred tank reactor

Maryam Amiraftabi, Mehdi Khiadani*, Hussein A. Mohammed

School of Engineering, Edith Cowan University, 270 Joondalup Drive, Joondalup, Perth, WA, 6027, Australia

ARTICLE INFO

Keywords:
Dual helical ribbon impeller
Gas-liquid stirred tank reactor
Power consumption
Mixing time
Bubble behaviour
Response surface methodology

ABSTRACT

The performance of a dual helical ribbon impeller in a gassed stirred tank reactor filled with a shear-thinning polymer has been investigated experimentally in this study. Sodium carboxymethyl cellulose with different concentrations were applied to change the viscosity and rheological behaviour of working fluid. Titration reaction between HCl and NaOH then took place inside the reactor under controlled pH, evaluating the influence of a dual helical ribbon impeller on the performance of a two-phase agitated reactor. The impact of impeller rotational speed, gas flow rate, viscosity, and clearance to the bottom on power uptake and mixing time are explored. The results thus reveal that the presence of bubbles reduces both required power uptake and mixing time to reach an endpoint reaction. Contrary to expectations, this study indicates that increasing the impeller's speed beyond a certain level, not only fails to further reduction in mixing time, whilst the power uptake increases exponentially.

Furthermore, for the first time, this study suggest that power number is inversely proportional to the square root of Reynolds number when systems are equipped with a dual helical ribbon impeller. The response surface method and quadratic numerical models are applied to suggest models in order to calculate the mixing time and power consumption.

1. Introduction

Stirred tank reactors (STRs[1]) are one of the most widely used pieces of equipment in process industries. Gas-liquid STRs are involved in many chemical and biochemical processes including various multiphase reactions, polymerization, fermentation, foam food processing, production of antibiotics, and digestion [1–6]. The efficient and cost-effective heat and mass transfer and homogeneity of dispersed phase and nutrients are the main objectives of these multiphase mixing processes [7]. To date, various methods have been developed and introduced to enhance the mixing performance of gas-liquid reactors that contain shear-thinning fluids [8–13]. An increase in rotational speed seems to be one promising method that prevents the development of unmixed regions, of forming nutrient segregations and non-uniformity of the dispersed phase. Although using a high rotational speed in some cases might reduce mixing times, it also reduces the productivity of microorganisms in biological units, and the performance of final products, where it similarly increases the operational costs of chemical processes. The main explanation for this limitation is that some materials and microorganisms are extremely shear-sensitive. For example, a high rotational speed disturbs the environment in which microorganisms seed and grow [11,12,14]. Microorganism cannot tolerate momentum, heat, and mass variations in their living environment, where high rotational speed or nonhomogeneous environments may consequently lead to switching metabolic pathways [7]. In cases where the shear sensitivity of substrate is an issue for reactor performance, using low rotational speed impellers has been suggested within the literature [14,15].

Using an ordinary small impeller including a Rushton turbine and pitched blade in a vessel filled with a non-Newtonian fluid has been shown to be inefficient and causes stagnant regions [16]. This phenomenon occurs because the central impeller fails to generate effective momentum and a sufficient shear rate in regions which are located far from the impeller itself. Close-clearance impellers including gate, anchor, screw and helical ribbon have been identified as ideal impellers by literature to complete mixing in a single-phase agitated systems involving non-Newtonian fluids [14]. Close-clearance impellers provide an almost tangential shear rate in the whole system, especially near the wall of the vessel which remains stagnant when non-Newtonian fluids rotate with an ordinary impeller [17]. In close-clearance agitator, the

* Corresponding author.
E-mail addresses: m.amiraftabi@ecu.edu.au (M. Amiraftabi), m.khiadani@ecu.edu.au (M. Khiadani), Hussein.mohammed@ecu.edu.au (H.A. Mohammed).

[1] Stirred Tank Reactor (STR)

https://doi.org/10.1016/j.cep.2020.107811
Received 7 September 2019; Received in revised form 17 December 2019; Accepted 9 January 2020
Available online 10 January 2020

Nomenclature

A	Cross sectional area (m^2)
AR	Aspect Ratio
D	Vessel inner diameter (m)
d	Impeller Diameter (m)
d_i	Impeller blade diameter (m)
d_s	Shaft diameter (m)
Flg	Gas flow number
g	Gravitational acceleration (m/s^2)
G_f	Gas Flow Rate (Lpm)
H	Depth of Fluid (m)
h	Impeller Height (m)
HCl	Hydrochloric Acid
IC	Impeller Clearance
K	Consistency Index ($Pa.s^n$)
K_s	Metzner and Otto's constant
$M_{Adjusted}$	Actual torque required to rotate the shaft (N.m)
$M_{display}$	Torque displayed by torquemeter (N.m)
$M_{friction}$	Friction torque (N.m)
N	Impeller Rotational Speed (rpm)
NaCMC	Sodium Carboxymethyl Cellulose
NaOH	Sodium hydroxide
Np	Power number (Dimensionless)
n	Flow index behaviour
P_0	Input power (W)
P_g	Power consumption after injection of gas (W)
Q_p	Upward pumping rate by fluid (Lpm)
Q_{AX}	Pumping rate by rising bubbles (Lpm)
Re	Reynold number (Dimensionless)
RSM	Response surface methodology
STR	Stirred Tank Reactor
u_g	Superficial gas velocity (m/s)
wt%	Weight percentage (%)
X	Variables
Y	RSM Response
β_0	RSM regression coefficients
β_i	RSM regression coefficients
β_{ii}	RSM interaction coefficient
β_{ij}	RSM interaction coefficient
γ_g	Gas shear rates (1/s)
γ_l	Liquid shear rates (1/s)
$\dot{\gamma}_T$	Average shear rates (1/s)
η	Average apparent viscosity (Pa.s)
ρ	Density (kg/m^3)
τ	Average shear stress (N/m^2)

high shear rate region is located between the wall and impeller blade, where the impeller sweeps wall and returns the stagnant volume of fluid into the bulk.

Power consumption and levels of homogeneity are two main factors affecting the design of an efficient reactor, have been investigated widely in the literature [7,14,16]. Power consumption determines the cost efficiency of using stirred tank reactors in process industries. Similarly, mixing time is an indicator of homogeneity in stirrers. Ameur and Bouzit [18] have indicated that a helical ribbon is the most efficient impeller, reducing mixing time when a fluid is shear-thinning. Delafosse et al. [19] have defined the mixing time as the time interval between the injection of the tracer and 95 % of the full homogeneity degree. They further indicated that the mixing time is a function of impeller geometry and tracer injection methods. The power consumption and mixing time have been investigated by Bao et al. [17], with different coaxial mixers for two different non-Newtonian fluids. The above author concluded that a combination of Paddler and helical ribbon impellers reduce the mixing time significantly.

To date, various methods including conductivity, thermal refractive index, redox ionic reaction, and decolouration have been developed and introduced to measure mixing time in agitated systems [20–25]. However, all of these techniques depend on the location of deliberately placed detectors, lights and cameras [26–28]. Titration has typically been applied as one of the most common techniques to evaluate mixing time in agitated vessels without any physical interference [27,28]. This non-intrusive technique has been used to measure the degree of homogenization and qualitatively to visualize the flow pattern including the formation of caverns, stagnant regions, and dead zones. Since the titration method is based on human observation, complementary approaches like the image processing method have been developed to reduce errors related to human eyesight [26,29]. Titration acid-base reaction has been used in this study to explore mixing times.

Apart from studies investigating the efficiency of agitators working in single-phase systems, there is a general lack of research on the performance of multiphase STRs filled with shear thinning fluid. Bouaif and Roustan [30] developed a dimensionless correlation between power consumption and mixing time in an aerated mixing system equipped with multi-impellers. Machon and Jahoda [31] have studied the effect of aeration on the mixing process in a multi-impeller vessel, where they concluded that aeration improves homogeneity and reduces the mixing time significantly. Further, Hashemi et al. [32] have measured bubble characteristics and gas holdup in mixing systems equipped with a combination of an anchor and central impeller. Some researchers have indicated that the presence of gas in gas-liquid systems enhances the homogeneity of the system and reduces mixing time [33–35]. Furthermore, many studies have shown that the gas flow rate and impeller speeds play a pivotal role in forming different flow patterns [36,37]. By changing the gas flow rate and rotational speed of an impeller, various flow patterns can be observed including flooding, loading, and complete dispersion [38,39]. In flooding pattern, gas bubbles rise quickly, thus the impeller speed fails to influence the bubble behaviour. The loading regime occurs when the gas flow rate decreases or the impeller speed increases. In this case, bubbles accumulate and become trapped behind the impeller or around the impeller shaft. The optimum scenario for gas-liquid systems is complete dispersion, where the gas bubble is well-distributed in the whole volume of the vessel [40]. A well-distributed mixing system holds bubbles inside for sufficient time in order to maintain bubbles and optimize heat and mass transfer [39].

A dual helical ribbon is a close-clearance impeller used in low Reynolds number under laminar and transient flow regimes to agitate shear sensitive non-Newtonian fluids. Dual helical ribbon impellers have been extensively studied in single-phase to evaluate the effect of geometry, rheology, kinematics (impeller speed), and impeller design on mixing time, homogeneity, and power uptake [41–47]. Chavan and Ulbrecht [47] have suggested a model based on geometry predicting power consumption for different types of helical ribbon impellers in the liquid phase. The influence of viscosity, viscoelasticity, and pseudoplasticity on the performance of an agitated system equipped with helical ribbon and helical ribbon screw impellers has been investigated by Brito-De La Fuente et al. [48]. They developed a model which indicates the deviation of pseudoplasticity from Newtonian power uptake for a helical ribbon impeller. Their findings are consistent with the general equation reported by Mentzor and Otto [41], although more research is needed to study the Mentzor- Otto correlation for strongly shear-thinning fluids.

Many reactions occur in gas-liquid phases, where, the presence of bubbles inside systems is unavoidable. Accordingly, researchers have shown an increased interest in the behaviour of bubbles and their influence on the flow pattern. Apart from Espinosa-Solares et al. [7] and

Cheng and Carreau [45] who have reported the influence of the presence of bubbles on power consumption of dual helical ribbons, previous studies are limited to single phase agitated systems. Therefore, little is known about the influence of impeller speed, gas flow rate, impeller clearance, and viscosity on mixing time and power consumption of multiphase agitated reactors driven by a dual helical ribbon impeller. Further, it is not clear how these factors are related to the desired mixing time and cost-effective power uptake when gassed STRs are filled with shear-thinning fluids. Additionally, there has been little information about the generalized correlation between power consumption and Reynolds number when a reactor tank is equipped with a dual helical ribbon impeller. Furthermore, little is known about the impacts of sparging gas into the system agitated with a helical ribbon impeller and it is not clear that rising bubbles has a positive or negative impact on the mixing performance.

Thus, the major objective of this study is to investigate the mixing performance of a helical ribbon impeller when the bubbles are dispersed, and the fluid phase is non-Newtonian. Further, this study evaluates the impacts of impeller speed, gas flow rate, impeller clearance from the bottom, and viscosity on mixing time and power consumption. It is believed that the empirical findings in this study would provide a new understanding of the flow pattern in the mixing process of gas-liquid STRs. The findings confirm that the association between impeller speed, gas flow rate, impeller clearance, and viscosity on the mixing time and power uptake. Data gathered from the experiments have identified that increases in impeller speed and gas flow rate are not always connected with reducing the mixing time and power consumption. Therefore, this study suggests a valuable correlation between Reynolds number and power number which remarkably influence the design, planning, and cost of gas-liquid reactors involving in process industries. The relationships between mixing time and power consumption with impeller speed, gas flow rate, impeller clearance, and viscosity have been suggested by ANOVA test. Therefore, the optimum response can be predicted in various operating conditions by using these two statistical equations achieved through response surface methodology (RSM[2]).

2. Materials and methods

2.1. Experimental setup

A transparent flat bottom and open-top cylindrical STR with an aluminium central shaft is studied, where the driven force of the stirrer is supplied by an electric motor. This type of system is widely used in mineral processing and oil storage. The[3] aspect ratio (AR: height to diameter) of the reactor has been determined to be 1.4. This ratio is kept in the range of 1–3 when an insoluble gas exists in the system where higher heat and mass transfer is the main requirement. The geometric configuration of the experimental set up is presented in Table 1 and shown in Fig. 1.

Gas flow was supplied at the bottom of the stirred tank equipped with a surface sparger consists of 10 equally spaced holes drilled on the periphery of the surface, each having a diameter of 0.00025 m. The compressed air is supplied to the system through a central air system and a flowmeter (Omega engineering flow meter with accuracy of ± 2 % Full Scale) with the range of 0–2.2 LPM is applied to control the airflow.

The calculated Reynolds number (Eq. 9) in the current experiment was between 10–1000, therefore, the flow regime was considered as a transient flow. While this study focuses on the transient regime, the combination of both laminar and turbulent flows exist in the system. This means that inertial forces dominate in turbulent regime, while viscous forces overcome in laminar flow.

In this study, NaCMC was used as working fluid due to its optical transparency and resistance to pH changes [49]. The reactor was filled up to 0.27 m of its height with NaCMC solution in four different concentrations of 0.1, 0.5, 1, and 1.5 wt%.

2.2. Acid-base reaction

Acid-Base titration reaction as an ordinary method of measuring the mixing time has been applied in this work for two different purposes [20–25]. The first one is to make it possible to see the evolution of colourful mixed region throughout the reactor as the impeller rotates. The second one is to find the mixing time by controlling the normality and volume of acid, base, and pH of the NaCMC solution. Adding the purple solution of NaOH and phenolphthalein into the agitated reactor followed by acid injection helps to visualize the chaotic movement of colour particles, homogenization process, and the formed vortices.

According to the previous study, to monitor fluid chaotic movement, 7 ml NaOH of 2 N and phenolphthalein indicator was injected closed the rotating shaft near the surface inside the reactor to raise pH value until the working fluid colour turns into purple in all regions. The reaction was recorded using a high-speed camera (Samsung digital Camera 12 M P with speed of 1.4 µm including dual-pixel autofocus) for further evaluation. Then, 5 ml of HCl solution was injected at the same location (near the impeller shaft) to decolourize the working fluid and the growth of decolouration of the working fluid was observed and recorded by the camera [20–25].

In this paper, mixing time is considered as the time taken for the 95 % of complete mixing where the solution was homogenous. Mixing time is determined by using RGB method and post processing software (ImageJ). This method is presented and described in literature in a systematic and detailed way [50,51].

Each experiment was repeated three times under the same conditions to ensure the consistency of the results. Additionally, the normality and volume of the required solution of acid and base were verified by titration before each set of experiments.

2.3. Torquemeters

The dissipated power of an impeller is correlated with impeller speed and rheological properties of liquid in which agitator is carried out. In this study, the power uptake by a mixing system was measured by a commercial torquemeter (GUNT system with ± 0.1 N.m). The consumed power and the adjusted torque were calculated from Eq. 11 and Eq. 12, respectively.

2.4. Rheometer

The viscoelastic characteristics of the polymer solutions was measured with a DHR-3, TA rheometer with normal accuracy ± 0.005, equipped with a coaxial cylinder cup with a diameter of 0.304 m, bob diameter of 0.28 m, bob height of 0.42 m, and gap distance of 0.001 m. Further, the temperature was controlled to 25 °C with a Peltier system during the tests.

Oscillation tests were carried out with increasing and decreasing ramp of strain from 1 to 300 % and vice versa at a constant frequency of 1 Hz in order to collect 30 points per decade. To remove the molecular network memory completely, the sample was pre-sheared at 300 s^{-1} up to 15 min, after loading the cup and reaching to the equilibrium stage. Then, this procedure was followed by a 5 min rest at zero shear rate [49].

2.5. Theoretical considerations

Flow regime, formation, and distribution of bubbles, and fluid rheological behaviour inside STRs are affected by the pumping rate of

[2] Response surface methodology (RSM)
[3] Aspect Ratio (AR)

Table 1
The geometric configuration of the stirred system.

Vessel inner diameter (m)	Vessel height (m)	Impeller height (m)	Impeller diameter (m)	Impeller blade diameter (m)	Impeller clearance (m)	Shaft diameter (m)
D	H	h	d	di	IC	ds
0.19	0.4	0.155	0.14	0.02	0.02, 0.04, 0.06	0.015

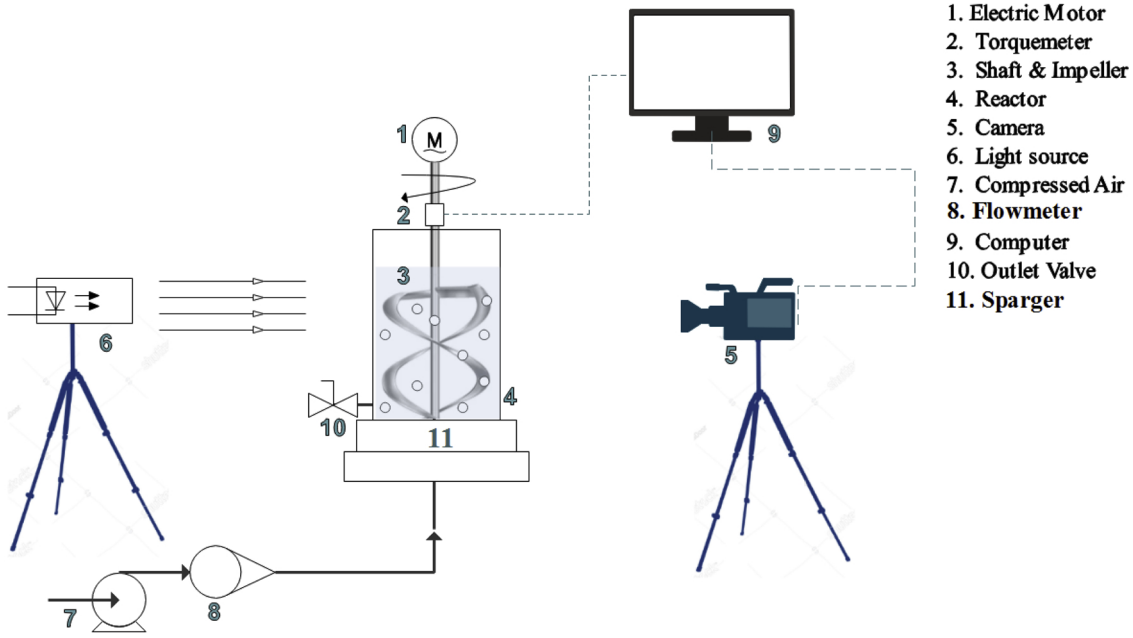

Fig. 1. Schematic of experimental setup.

the agitator which Q_p[4] is upward pumping rate by fluid (Lpm) and Q_{AX}[5] is the volume rate of liquid pumping upwards by rising bubbles (Lpm) [34]. Smith [34] has suggested the following two equations to predict the flow regime of gas-liquid agitated systems. If $Q_{AX} \neq Q_p$, the reactor flow pattern in loading/ flooding transition is not desirable.

$$Q_{AX} \propto (G_f g H^5) \tag{1}$$

$$Q_p \propto (Nd^3) \tag{2}$$

where H is the depth of fluid in the reactor (m), G_f is the gas flow rate (LPM), D is the diameter of impeller (m), N is the impeller rotational speed (rpm), and g is the gravitational acceleration constant (m/s^2).

This study examines Q_p and Q_{AX} for various impeller speeds and different gas flow rates combined with visual observation in order to assure the flow regime undergoes complete dispersion inside the reactor.

In gas-liquid agitation reactors, the maximum shear rate is imposed by the rotary mechanical part. However, rising gas bubbles can also have some impact on the fluid bulk. In this case, the average total shear rate can be calculated from;

$$\dot{\gamma}_T = \sqrt{\dot{\gamma}_g^2 + \dot{\gamma}_i^2} \tag{3}$$

where, $\dot{\gamma}_i$ is liquid shear rates (1/s), $\dot{\gamma}_g$ is gas shear rates (1/s), and $\dot{\gamma}_T$ is average total shear rates (1/s).

According to Metzner and Otto's correlation [52] the average shear rate for shear-thinning fluids inside an agitated system ($\dot{\gamma}_i$) can be defined as follows:

$$\dot{\gamma}_i = K_s N \tag{4}$$

where $\dot{\gamma}_i$ is the average shear rate in a stirred vessel depending on the impeller geometry and characteristics reflecting in Mentzer and Otto's constant (K_s) [52]. Additionally, the strong dependency of K_s to fluid rheology has been widely investigated in the literature. Some researchers have indicated that flow index behaviour (n) is proportional to K_s [53], while others report the decreasing value of K_s is correlated to increasing flow index behaviour [54,55].

Additionally, the gas shear rates (γ_g) can be calculated by Hashikawa's correlation [56], which shows the effect of bubble motion on liquid and defined as;

$$\dot{\gamma}_g = 1500 u_g \tag{5}$$

$$u_g = \frac{G_f}{A} \tag{6}$$

where u_g is the superficial gas velocity (m/s) which is consider equal to 1500 m/s as a proportional constant and A is Cross sectional area (m^2).

η[6] is the average apparent viscosity (Pa.s) and can be calculated by the correlation between the $\dot{\gamma}_T$ and τ[7] as a shear stress (N/m^2).

$$\eta = \tau / \dot{\gamma}_T = \frac{\tau}{\sqrt{(K_s N)^2 + (1500 u_g)^2}} \tag{7}$$

Further, a previous study noted NaCMC as a shear-thinning fluid that follows the Power-Law equation [49].

$$\tau = K \dot{\gamma}_i^n = K (K_s N)^n \tag{8}$$

where n is the flow index, K is the consistency index (Pa.s^n). All these rheological parameters have been investigated in a previous study [49], where the rheological factors for NaCMC are summarized in Table 2.

Eq. 9 shows the Reynolds number for a stirred system. Substitution of the Power-Law model in Eq. 8 leads to obtaining Reynolds number for a dual helical ribbon. Fuente et al. [48] have reported K_s = 32.9–35.7 for a dual helical ribbon impeller in a shear-thinning fluid, whereas n is close to 1.

Table 2
The rheological parameters of NaCMC [49].

Concentration (wt%)	n (-)	K (Pa.s^n)
0.1	0.98	0.08
0.5	0.92	0.13
1	0.82	0.46
1.5	0.58	4.3

$$Re = \frac{\rho N d^2}{\eta} \tag{9}$$

In most recent studies, the mixing time as an indicator of homogeneity has been measured in different approaches including local and general mixing time [57]. Within the realm of macromixing, bulk mixing time t(s) is the time taken for the complete mixing, where the solution is homogenous.

The Power number represents the rate of energy dissipation within the liquid and the power consumption by impeller in a specific rotational speed. Ungassed power number as the most important parameters in coaxial mixers have been studied widely [58,59].

$$N_p = \frac{P_0}{\rho N^3 d^5} \tag{10}$$

where ρ is density (kg/m^3).

P_0 as input power (W) is one of the main parameters evaluating the efficiency of ungassed impeller which can be calculated by using the following formula [60–62]:

$$P_0 = 2.\ \pi.\ N.\ M_{Adjusted} \tag{11}$$

Furthermore, Bourne and Butler [63] have proven that there is a correlation between Reynolds number and Power number in single phase viscose fluid. Finally, torque should be obtained from the following formula:

$$M_{Adjusted} = M_{display} - M_{friction} \tag{12}$$

$M_{Adjusted}$[8] is the actual torque required to rotate the shaft (N.m). It can be calculated from the subtracting the friction torque ($M_{friction}$[9]) from what is monitored on the power meter ($M_{display}$[10]) (N.m). If the impeller rotates in the open air, the magnitude of torque will be considered as friction torque.

2.6. Response surface method

Response surface method (RSM) approach was used to predict the mixing time and power consumption under different operating conditions. The main objective of the RMS is e to identify the correlation between variables including impeller speed, gas flow rate, impeller clearance, and viscosity as well as responses including mixing time and power consumption. For this purpose, the Box-Behnken method is used to design the experiments. Next, the response surface methodology (RSM) is applied to optimize the factor levels and find the most influential parameters. For each experiment, three replicates are considered to ensure the reproducibility of the experiments. The correlation is defined as:

$$Y = \beta_0 + \sum_{i=1}^{3} \beta_i X_i + \sum_{i=1}^{3} \beta_{ii} X_i^2 + \sum_{i=1}^{3} \sum_{j=2}^{3} \beta_{ij} X_i X_j + error \tag{13}$$

[4] Upward pumping rate (Q_p)
[5] Volume rate of liquid pumping upwards (Q_{AX})
[6] Average apparent viscosity (η)
[7] Shear stress (τ)
[8] Actual torque required to rotate the shaft ($M_{adjusted}$)
[9] Friction torque ($M_{friction}$)
[10] Torque displayed by torquemeter ($M_{display}$)

Table 3
Variables used in RSM method to optimize the mixer performance and uncertainty analysis for different variables.

Symbols	Variables	Low level	Central level	High level	Instrument	Systematic Uncertainty (± %)	Random Uncertainty (± %)	Total Uncertainty (± %)
X_1	Impeller speed (1/s)	50	75	100	Torquemeter	–	1	1.00
X_2	Gas flow rate (Lpm)	0.5	1.35	2.2	Flow meter	1.5	0.66	1.64
X_3	Impeller clearance (m)	0.02	0.04	0.06	Ruler	0.5	0.83	0.97
X_4	Concentration (wt %)	0.1	0.8	1.5	Scale	0.1	0.32	0.34

In this equation, X shows variables, Y indicates the response such as mixing time, while β_0[11], β_i[12], β_{ii}[13], and β_{ij}[14] are regression coefficients and interaction terms. Different 3D surface plots are plotted to find the most influential factor when the other factor are at optimized level [64].

The list of variables and their maximum and minimum levels are summarized in Table 3. These maximum and minimum levels are selected based on the preliminary study.

Further, uncertainty analysis has been done for measured and calculated data, as well as instrument accuracy. The result of uncertainty analysis is summarized in Table 3.

3. Results and discussion

In this study, the impeller speed, gas flow rate, impeller clearance from the bottom, and viscosity are considered as principal factors influencing the mixing process of a shear thinning fluid. It is worth noting that the maximum impeller speed in the current investigation was limited to 100 rpm. This limitation was considered because of the extreme shear sensitivity of some materials and microorganisms [11,65].

As mentioned earlier, the experiments were carried out in the optimal range where the hydrodynamics of a gas-liquid system is completely dispersed. The influence of gas flow rates of 0.5–2.2 Lpm is examined when the system is agitated by a dual helical ribbon impeller between 50–100 rpm under transient flow regime. Generally, the effects of bubble motion, impeller speed, gas flow rate, and viscosity on power consumption and mixing time are discussed and interpreted in this section.

3.1. Mixing pattern

The two-dimensional cross-section of the mixing pattern in the vessel when the reaction between acid and base occurs is shown in Fig. 2.

The visual evidence presented in this section shows that initially, the radial movement of fluid bulk is stronger than the axial movement for a dual helical ribbon. The impeller drives fluid towards the walls of the vessel where the shear rate is at the maximum, where little movement of fluid can be observed in the axial direction near the central shaft. Then, fluid moves downward alongside the cylinder wall. Following this, the axial movements become stronger and the top surface becomes clear. Decolouration of the purple fluid shows that the maximum mixing in this type of impeller happens close to the clearance between the wall and impeller where the high shear imposes on the fluid film as well as areas near to the inner edge of the blade. Whilst, there is still an unmixed zone located at the bottom of the tank, the efficiency of the impeller in the region near the wall is significant. Therefore, the mixing time is controlled by the mixing pattern of the low-shear central regions located far from the blade edges. A possible explanation for these results may be the reduction in viscosity when the high shear rate region rotates near the inner and outer edges of the blade. The enclosed volume of fluid between impeller and wall as well as the bulk of fluids around the inner edge of the blade can be considered as a low viscosity film which can be easily influenced by this type of impeller. Generally, these regions are introduced as a stagnant zone in other types of impellers.

Although extensive research has been carried out on the effects of dual helical ribbon impellers on single phase flow pattern, few studies have paid attention to the influence of chaotic bubble motion on multi phases mixing process [56]. Fig. 3 indicates the qualitative mixing pattern over time when air bubbles are introduced. Rising a bubble from bottom of the tank imposes shear rate to the bulk of the fluid. As a result, the viscosity of the shear-thinning fluid is reduced to some extent depending on the gas flow rate, general gas hold-up, and rheology of the fluid. The more reduction in viscosity, the more desirable results are achieved including less energy consumption and shorter mixing time. Since bubbles are dispersed everywhere, the mixed area near the central shaft can gradually develop, which enhances the mixing performance of the dual helical ribbon impeller.

Fig. 3 indicates that in a low rotational speed helical ribbon impeller, the formed bubbles rise without significant breakage or coalescence. They are trapped behind the impeller blade and form a film of gas which follows the impeller patterns to reach the free surface. The interesting point here is the enhancement of the uniformity of homogenization and dispersion of liquid inside the system. In the presence of bubbles, after the injection of acid, clear liquid not only moves toward the clearance of the vessel and impeller but also gradually penetrates downward. Although this requires more investigation, this phenomenon could be interpreted by increasing the internal liquid shear stress as a result of bubbles motions. In completely disperse mixing patterns, bubbles disperse completely in the whole system, even in stagnant regions. The presence of bubbles in the stagnant zones increases the shear stress resulting in the breakdown of the NaCMC internal network [49]. Weakening the network structure of shear-thinning fluids increases both molecular and bulk diffusions resulting in enhancement of the mixing process.

3.2. Impact of impeller speed

The impact of various rotational speeds on the performance of the mixing system has been studied widely in the literature. Results show that an increase in rotational speed reduces the time of mixing and improves the homogeneity of heat, mass, and nutrient [7,10,37,66,67].

Fig. 4a and b depict both mixing time and power consumption over various rotational speeds for different concentration of NaCMC solutions. The results indicate that a higher rotational speed leads to shortened mixing time, while power uptake increases exponentially. The results indicate that an increase in rotational speed up to 75 rpm could reduce the mixing time of viscous fluid to some extent.

Fig. 4a shows the expected time to reach homogeneity in different impeller rotational speeds. For the same rotational speed, the more concentrated solution the more time required to reach homogenous conditions, where the natural gel structure of polymer requires more energy and time to destroy. Therefore, the diluted solution requires less time in a lower rotational speed to reach a certain level of homogeneity. Further, it can be noted that the homogeneity graphs are exponential

[11] RSM regression coefficients (β_0)
[12] RSM regression coefficients (β_i)
[13] RSM interaction coefficient (β_{ii})
[14] RSM interaction coefficient (β_{ij})

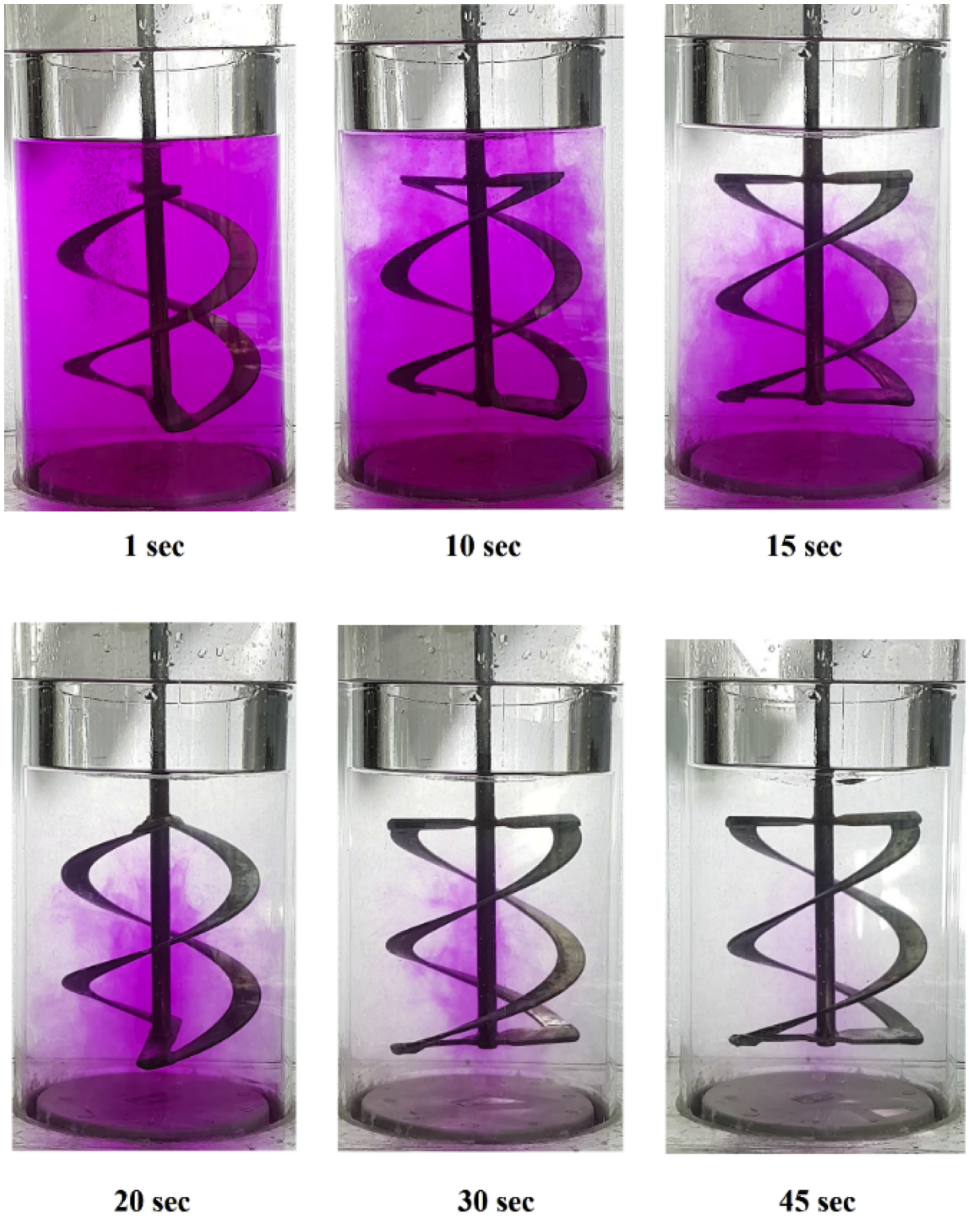

Fig. 2. The evolution of mixed area inside the reactor when the impeller speed is 75 rpm and concentration of NaCMC solution is 1 %.

which become level off at the end. Thus, it seems that the system has become homogenous in somewhere between rotational speed of 0 − 50 rpm when the concentration of NaCMC solution is 0.1 %.

However, increasing the rotational speed beyond 75 rpm not only has insignificant contribution in reducing the mixing time but also exponentially increases power consumption. This finding suggests that increasing the impeller speed up to optimum value could enhance the performance of the mixing system. Whilst, after this certain level, the power consumption increases sharply with a limited positive contribution to mixing performance.

Two different dimensionless terms have been defined to investigate the extra power consumed by the impeller compared to mixing time reduction. The first term is the extra power consumed when the impeller speed increases from 75 to 85 and 100 rpm and the second term is the decrease of the mixing time when the impeller speed increases to 85 and 100 rpm.

Fig. 5 represents these two dimensionless terms for different concentrations of NaCMC. According to this figure, a remarkable increase is observed in the percentage of power uptake compared to the reduction in the percentage of mixing time when the solution is more concentrated. For example, when impeller speed changes from 85 to 100 rpm in a concentration of 1.5 % solution, the power consumption has been increased by 60 %, while the mixing time decreased by 10 %. This finding is vital in terms of cost efficiency and scaling up the system.

3.3. Influence of bubble motion

The mixing time versus gas flow rate for gassed cases in both stirred and non-stirred conditions is shown in Fig. 6. Hollow markers show the mixing time in different gas flow rates for various concentrations of NaCMC solutions when the impeller speed is 75 rpm. Filled markers demonstrate the mixing time under the same operating conditions when the impeller is off (impeller speed = 0 rpm). The results in this figure reveal that the gas flow rate is an influential factor in mixing time when

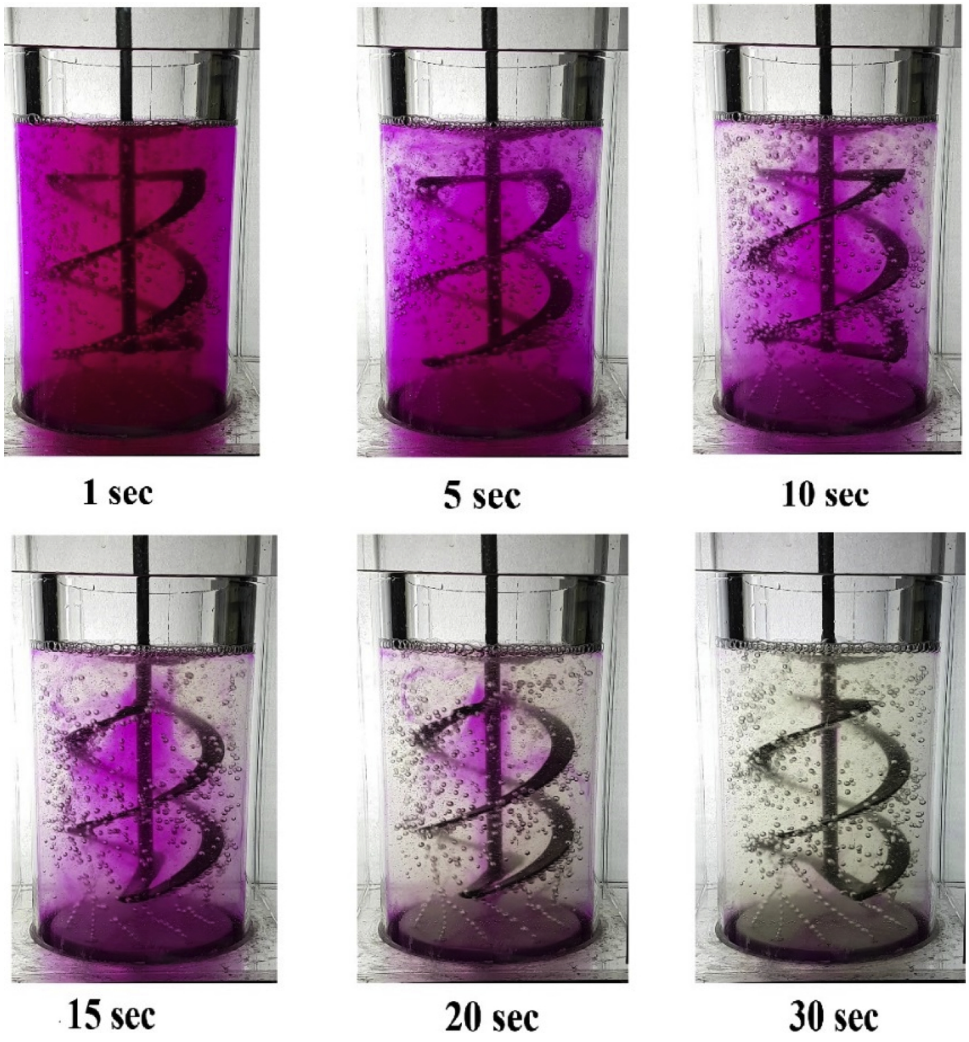

Fig. 3. The evolution of mixed area inside the aerated reactor when the impeller speed is 75 rpm and concentration of NaCMC solution is 1 %.

the mechanical agitator is not working. Increasing the gas flow rate from 0.5 to 2.2 LPM could reduce the mixing time to half in non-stirred systems. However, hollow markers show that the mechanical agitator is more influential on mixing time compared to the gas flow rate.

Some previous studies suggest that for a system with a Rushton turbine and PBD- anchor, the gas flow rate increases the mixing time [36,37]. It has been argued that in high gas flow rate, the buoyancy force overcomes the hydrodynamics of system and the gas-liquid system flooded [36,37]. Other researchers, however, have reported an improvement in the mixing performance by the presence of bubbles inside the system [33–35]. This inconsistency may be due to the complex hydrodynamics of gas-liquid agitated flow patterns. The variety of hydrodynamics in gas-liquid STRs can be almost considered as a function of impeller type, rheology of fluid, gas flow rate, impeller speed, and bubble size [39].

3.4. Power consumption

Power uptake is another influential design parameter representing the economic performance of a mixing system. The power consumption of the impeller should be taken into account when the cost efficiency of a mixing process is important. Power consumption displays the performance of the agitating process depending on the geometry of impeller and physical properties of the fluid [68]. The power consumption measurement has been carried out on NaCMC solution with different concentrations of 0.1, 0.5, 1, and 1.5 wt% for five different impeller speeds of 50, 65, 75, 85, and 100 rpm.

Fig. 7a indicates the power uptake by impeller versus Reynolds number for the rotational speed of 50, 65, 75, 85, and 100 rpm for different concentration of NaCMC solutions. The greater the viscoelasticity of the fluid, the greater the energy required to achieve complete mixing. It can be observed that an increase in viscosity shifts the power curve to the lower Reynolds numbers and higher energy consumption.

Fig. 7b displays the dimensionless energy consumption (N_p) as a function of Reynolds number (Re) or power curve for a dual helical ribbon in five different rotational speeds of 50, 65, 75, 85 and 100 rpm and constant gas flow rate of 1 LPM. The power curve is unique for each impeller type. The single most striking observation to emerge from the plotted data is the relationship between N_p and Re, which for the first time this result has been presented. Regression analysis was used to predict the correlation between these two parameters which is importantly repeated for all concentrations of NaCMC, whereas the flow regime is transient. This practical correlation has been reported in Eq. 14. It is noticed that this practical correlation is unique and demonstrating how a dual helical ribbon impeller performs in a transient two phases flow regime.

$$N_p.\ Re^{\beta} = \alpha \text{ or } N_p = 918.9Re^{-0.5} \tag{14}$$

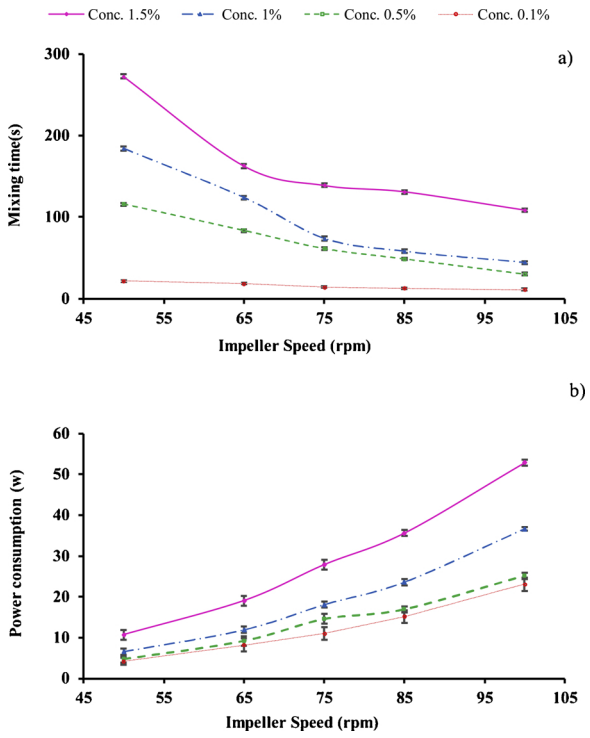

Fig. 4. a) Mean mixing time and b) mean power consumption with error bars over impeller speed in different concentration of NaCMC solutions.

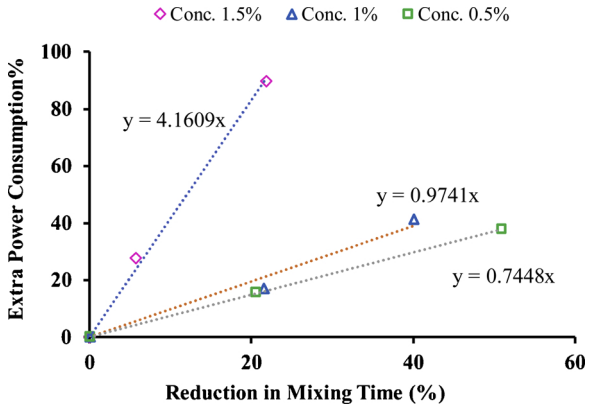

Fig. 5. Comparison between the percentage of power consumption and percentage of enhancing mixing time.

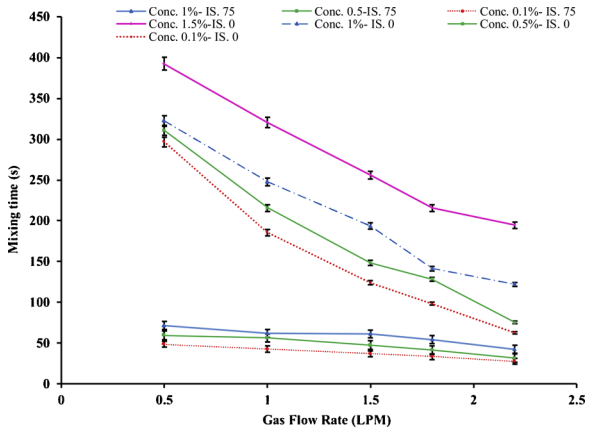

Fig. 6. Comparison between the mean gassed mixing time with error bars in both stirred and non-stirred conditions.

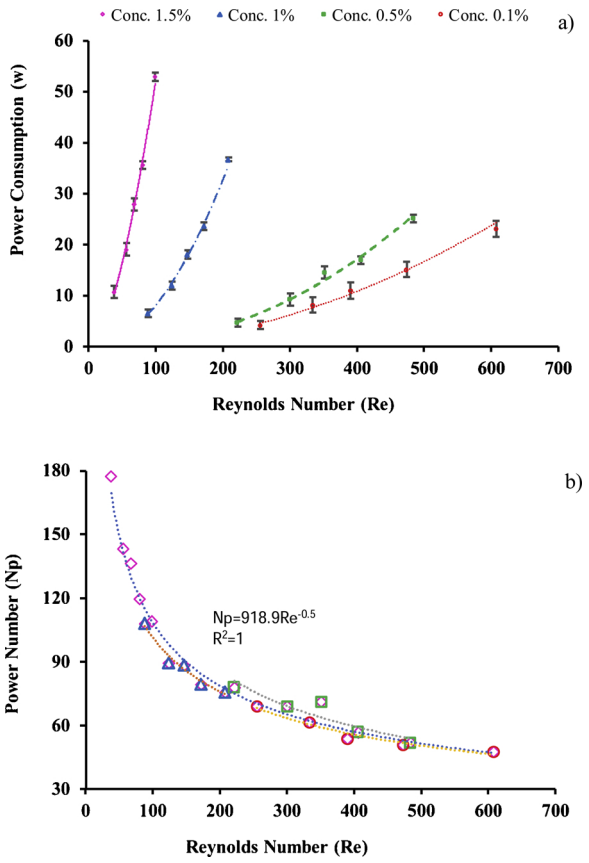

Fig. 7. a) Mean power curve and b) Power number (Np) vs. Reynolds number (Re) for a dual helical ribbon in five different rotational speeds for various concentrations of NaCMC.

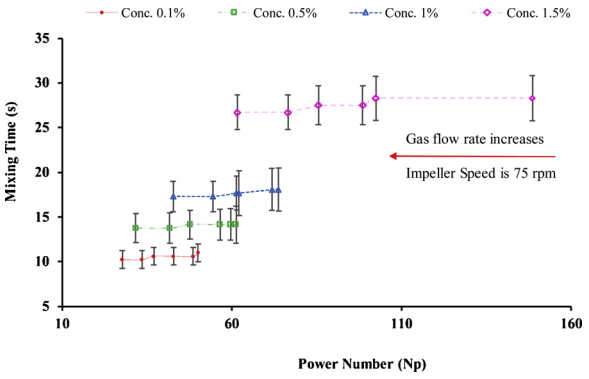

Fig. 8. Influence of gas injection on mean mixing time with error bars over power number (Np).

where, $\beta = 0.5$ and $\alpha = 918.9$ are constant for a dual helical ribbon impeller in different concentration of NaCMC solutions from 0.1 wt% to 1.5 wt%.

What is surprising here is that the trend of the power curve is not influenced by changes in concentration. Patel et al. [69] have indicated that $Re.N_p$ is a constant value for the Scaba and the A320 impellers in single-phase flow. They also mentioned that the power number changes slightly based on Reynolds number in transient flow for the Scaba and the A320 impeller in single-phase flow. However, this correlation has not previously been found for a dual helical ribbon impeller in gas-liquid interactions.

Additionally, Fig. 8 shows the power consumption as a function of mixing time at a constant impeller speed of 75 rpm. These results show the effect of bubble motion on mixing time and power consumption.

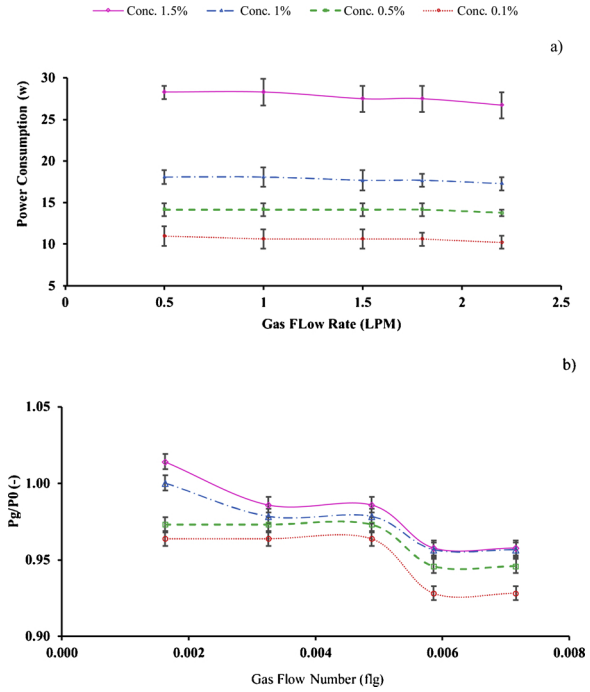

Fig. 9. The role of bubble motion around the impeller on mean power consumption.

Interestingly, a decrease in power consumption was observed when gas was injected into the system. This 5–7 % reduction in power consumption could be due to the presence of bubbles inside the reactor. The reduction in power uptake by sparging bubbles in a mixing system has also been observed by other researchers [30,70]. This finding can be interpreted through the formation of gas pockets (cavities) underneath the impeller streamlining the blade movement and reducing fluid drag resulting in lower power consumption. Further, reducing the viscosity of shear thinning fluid as a result of axial and rotational bubble movements can be considered as another influential factor.

In addition, Fig. 8 depicts that both power consumption and mixing time are highly affected by the viscosity of the fluid. The higher the viscosity of the fluid, the more power required to achieve complete mixing. Therefore, when the viscosity of the shear-thinning fluid increases, more power and time are required to achieve desirable mixing.

These results differ from most published studies that reported bubble motion causes an increase in power consumption of an aerated stirred system [30,70]. However, the present results are in agreement with Cheng and Carreau's [45] findings which show the presence of bubbles leads to a reduction of power consumption by the impeller.

Fig. 9a and b clearly describes the role of gas flow rate on power consumption where the impeller rotational speed is constant at 75 rpm. According to Fig. 9a, an increase in gas flow rate from 1 to 2.2 LPM reduces the mixing power to some extent. Further Fig. 9b, represents the ratio of power uptake by impeller when the gas sparged (Pg), watt,

Table 5
Results of ANOVA test for Quadratic model.

Response	Mixing time		Power consumption	
Source	F-value	P-value	F-value	P-value
Model	45.37	< 0.0001*	128.1	< 0.0001*
A-Impeller Speed	14.52	0.0034*	1138.3	< 0.0001*
B-Gas Flow rate	151.38	< 0.0001*	0.4454	0.5197 ns
C-Concentration	379.81	< 0.0001*	513.47	< 0.0001*
D-Impeller Clearance	13.54	0.0042*	0.1121	0.7447 ns
AB	0.0182	0.8953 ns	0.016	0.9019 ns
AC	12.17	0.0058*	82.98	< 0.0001*
AD	5.29	0.0442*	0.3362	0.5749 ns
BC	4.96	0.051 ns	0.1891	0.6729 ns
BD	0.0127	0.9126 ns	0	1 ns
CD	0.8933	0.3669 ns	0	1 ns
A^2	2.48	0.1466 ns	20.95	0.001*
B^2	2.95	0.1165 ns	0.0326	0.8603 ns
C^2	12.92	0.0049*	19.56	0.0013*
D^2	0.2279	0.6433 ns	0.206	0.6596 ns

*: Not significant at P < 0.05, ns: Significant at P > 0.05.
P – value and F – value: Indicator of significance decision.

Table 4
Plan for ANOVA analysis.

Order	Impeller speed (N)	Gas flow rate (Gf)	Impeller Clearance (IC)[a]	Concentration (C)	Mixing Time	Power consumption
	rpm	LPM	m	wt%	s	W
1	100	0.5	0.04	0.8	57	30.8
2	75	0.5	0.04	1.5	102.4	27.88
3	75	1.35	0.02	0.1	34	10.6
4	75	0.5	0.04	0.1	48.7	10.6
5	75	1.35	0.06	0.1	45.5	10.6
6	75	1.35	0.06	1.5	91.1	27.1
7	75	0.5	0.02	0.8	65.5	16.3
8	75	2.2	0.04	0.1	27.8	10.2
9	75	1.35	0.02	1.5	88	27.1
10	50	1.35	0.06	0.8	63.25	6.5
11	75	2.2	0.02	0.8	31.5	15.3
12	50	1.35	0.02	0.8	42.8	6.5
13	100	1.35	0.04	1.5	95.8	52.8
14	75	2.2	0.06	0.8	42.8	15.3
15	75	0.5	0.06	0.8	75.8	16.3
16	100	1.35	0.06	0.8	46.5	32.46
17	75	1.35	0.04	0.8	57.1	15.1
18	50	2.2	0.04	0.8	39	6.54
19	50	1.35	0.04	0.1	49.8	4.45
20	75	2.2	0.04	1.5	61.7	26.31
21	100	1.35	0.04	0.1	23.9	20.94
22	100	2.2	0.04	0.8	26	31.4
23	50	0.5	0.04	0.8	68.8	6.28
24	100	1.35	0.02	0.8	46.5	30.9
25	50	1.35	0.04	1.5	90.7	11.8

[a] Impeller Clearance (IC).

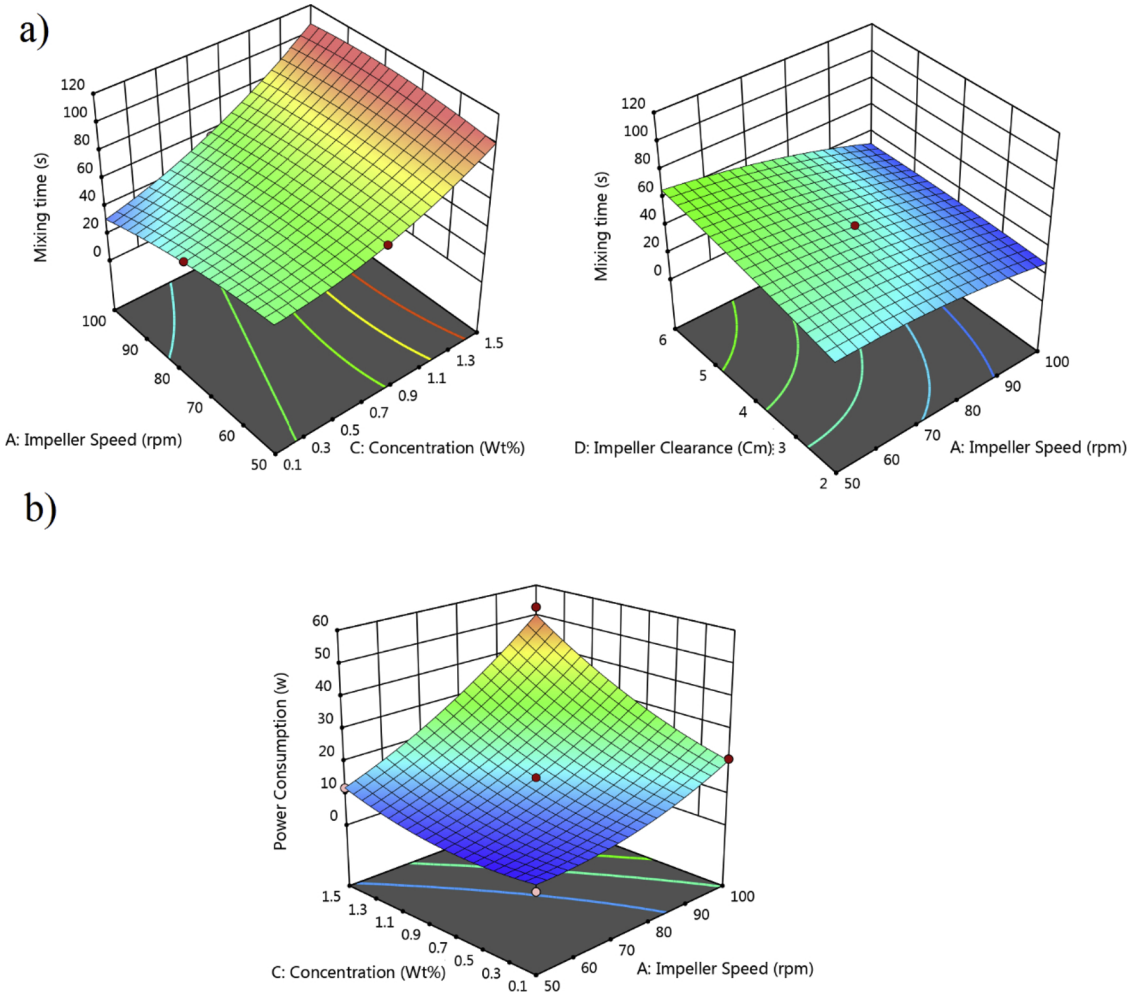

Fig. 10. Influential interaction model parameters analysed by ANOVA test.

to the power consumption of single-phase system (P_0), watt, over the gas flow number (flg[15]) which shows the flow developing in the impeller zone independent to impeller geometry.

This figure shows that power consumption experiences a significant fall after a certain value of gas flow rate. Dispersed bubbles can reduce the viscosity of the fluid around the blade to some extent and reduce the power uptake. By increasing the impeller speed, the bubbles disperse everywhere in the fluid bulk and some of them still follow the impeller path. As a result, the impeller has the maximum level of contact with the air bubbles trapped behind the blade which slightly decrease the power consumption of the aerated system compared to single-phase one.

3.5. Statistical analysis

This proposed study investigates the impacts of four listed factors shown in Table 3 through the three-level Box-Behnken method [71]. Then, the response surface methodology (RSM) is applied to optimize and to find the most influential factors and their interactions. Table 4 summarizes the plan, the number of experiments and variables applied in RSM.

The result of statistical analysis suggests strong correlations between responses and all independent and dependent variables lead to Eq. 15 and Eq. 16.

$$\begin{aligned} \textit{Mixing time} = & -1.26 + 0.88\,N + 5.5\,Gf - 11.31\,C + 13.56\,IC \\ & - 0.014\,N \times Gf + 0.44\,N \times conc. - 0.1\,N \times IC \\ & - 8.3\,Gf \times conc. + 0.14 Gf \times IC - 1.5\,Conc. \times IC \\ & + 0.0067\,N^2 - 6.3\,Gf^2 + 19.4\,C^2 - 0.32\,IC^2 (\text{Adjusted R2} \\ & = 0.9628) \end{aligned} \tag{15}$$

$$\begin{aligned} \textit{Power Consumption} = & \ 28.53 - 0.67\,N - 0.75\,Gf - 1.25\,IC - 24.58\,C \\ & + 0.004\,N \times Gf + 0.35\,N \times C + 0.007\,N \times IC \\ & - 0.49 Gf \times C + 3.9E^{-16} Gf \times IC - 1.07^{-15} C \times IC \\ & + 0.0058\,IS^2 + 0.2\,Gf^2 + 7.23\,C^2 \\ & + 0.09\,IC^2 (\text{Adjusted R2} = 0.9867) \end{aligned} \tag{16}$$

where N is the impeller speed, Gf is the gas flow rate, C is the concentration of the solution, and IC is the impeller clearance.

Further, the result of ANOVA test has been summarized in Table 5 for the response surface quadratic model. This table demonstrates P-values and F-values for all variables. In this case, A, B, C, D, AC, AD, BC, A^2, and C^2 are significant model parameters.

The Model F-values of 45.37 for mixing time and 128.1 for power consumption confirm that the proposed Eq. 14 and Eq. 15 are reliable and remarkably accurate to predict the mixing time and power consumption in different operating conditions. These equations have significant practical value for industrial designing, operating, and cost studying of STRs.

To sum up, the statistical analysis indicates that impeller speed, gas

[15] Gas flow number (flg)

flow rate, impeller clearance, and viscosity influence the mixing time and power consumption, respectively.

Further, analysis of interactions between variables and the model coefficients are displayed in three-dimensional response surfaces and are shown in Fig. 10a, b. This figure displays the significant interaction model parameters based on P-value < 0.05. Fig. 10a shows the most influential interactions on mixing time including impeller speed-concentration, and impeller clearance-impeller speed. Additionally, according to P-value, the most influential model parameter on power consumption is interaction of concentration-impeller speed as shown in Fig. 10b.

4. Conclusions

Collectively, this study outlines the role of a helical ribbon impeller on mixing performance and cost of operation of a gassed STR. The range of gas flow rate and impeller speed has been adjusted in the preliminary study. In addition, this work provides a conceptual understanding of the flow pattern inside a gassed reactor equipped with a dual helical ribbon impeller and filled with a shear thinning fluid. The findings of this study suggest that increasing the rotational speed more than 75 rpm not only fails to reduce mixing time but also increases the power consumption. It can be concluded that the optimum rotational speed should be selected with caution because boosting impeller speed may impose the extra operating cost while the efficiency of mixing remains unchanged. Additionally, aeration enhances power uptake and mixing time to some extent. Further, based on the experimental data in this study, two equations are proposed using ANOVA test to predict the mixing time and power uptake for a helical ribbon impeller in different operating conditions. The statistical analysis demonstrates the significant role of viscosity and impeller speed on the mixing performance. Suggesting a practical correlation between Reynolds and power numbers, this study provides unique and valuable results that can be applied to process industries.

Declaration of Competing Interest

The authors declare that there are no conflicts of interest.

Appendix A. Supplementary data

Supplementary material related to this article can be found, in the online version, at doi:https://doi.org/10.1016/j.cep.2020.107811.

References

[1] L. Samandari-Masouleh, N. Mostoufi, A. Khodadadi, Y. Mortazavi, M. Maghrebi, Modeling the growth of carbon nanotubes in a floating catalyst reactor, Ind. Eng. Chem. Res. 51 (2012) 1143–1149, https://doi.org/10.1021/ie201137j.

[2] L. Samandari-Masouleh, N. Mostoufi, A.A. Khodadadi, Y. Mortazavi, M. Maghrebi, Kinetic modeling of carbon nanotube production and minimization of amorphous carbon overlayer deposition in floating catalyst method, Int. J. Chem. React. Eng. 10 (2012) 10–12, https://doi.org/10.1515/1542-6580.2972.

[3] S. Miryahyaei, K. Olinga, F.A. Abdul Muthalib, T. Das, M.S. Ab Aziz, M. Othman, J.C. Baudez, D. Batstone, N. Eshtiaghi, Impact of rheological properties of substrate on anaerobic digestion and digestate dewaterability: new insights through rheological and physico-chemical interaction, Water Res. 150 (2019) 56–67, https://doi.org/10.1016/j.watres.2018.11.049.

[4] M. Schrimpf, J. Esteban, T. Rösler, A.J. Vorholt, W. Leitner, Intensified reactors for gas-liquid-Liquid multiphase catalysis: from chemistry to engineering, Chem. Eng. J. 372 (2019) 917–939, https://doi.org/10.1016/j.cej.2019.03.133.

[5] F. Almeida, F. Rocha, A. Ferreira, Analysis of liquid flow and mixing in an oscillatory flow reactor provided with 2D smooth periodic constrictions, U. Porto J. Eng. 4 (2018) 1–15, https://doi.org/10.24840/2183-6493_004.002_0001.

[6] E.K. Nauha, Z. Kálal, J.M. Ali, V. Alopaeus, Compartmental modeling of large stirred tank bioreactors with high gas volume fractions, Chem. Eng. J. 334 (2018) 2319–2334, https://doi.org/10.1016/j.cej.2017.11.182.

[7] T. Espinosa-Solares, E. Brito-De La Fuente, A. Tecante, L. Medina-Torres, P.A. Tanguy, Mixing time in rheologically evolving model fluids by hybrid dual mixing systems, Chem. Eng. Res. Des. 80 (2002) 817–823, https://doi.org/10.1205/026387602321143345.

[8] L. Pakzad, F. Ein-mozaffari, S.R. Upreti, A. Lohi, Chemical engineering research and design agitation of Herschel – bulkley fluids with the Scaba – anchor coaxial mixers, Chem. Eng. Res. Des. 91 (2012) 761–777, https://doi.org/10.1016/j.cherd.2012.09.008.

[9] L. Pakzad, F. Ein-Mozaffari, S.R. Upreti, A. Lohi, Characterisation of the mixing of non-newtonian fluids with a scaba 6SRGT impeller through ert and CFD, Can. J. Chem. Eng. 91 (2013) 90–100, https://doi.org/10.1002/cjce.21616.

[10] L. Pakzad, F. Ein-Mozaffari, P. Chan, Measuring mixing time in the agitation of non-Newtonian fluids through electrical resistance tomography, Chem. Eng. Technol. 31 (2008) 1838–1845, https://doi.org/10.1002/ceat.200800362.

[11] D.J. Lamberto, F.J. Muzzio, P.D. Swanson, A.L. Tonkovich, Using time-dependent RPM to enhance mixing in stirred vessels, Chem. Eng. Sci. 51 (1996) 733–741, https://doi.org/10.1016/0009-2509(95)00203-0.

[12] T. Espinosa-Solares, E. Brito-De La Fuente, A. Tecante, P.A. Tanguy, Power consumption of a dual turbine-helical ribbon impeller mixer in ungassed conditions, Chem. Eng. J. 67 (1997) 215–219, https://doi.org/10.1016/S1385-8947(97)00040-5.

[13] M.S. Amiraftabi, N. Mostoufi, M. Hosseinzadeh, M.R. Mehrnia, Reduction of membrane fouling by innovative method (injection of air jet), J. Environ. Health Sci. Eng. 12 (2014) 1–8, https://doi.org/10.1186/s40201-014-0128-0.

[14] J. Jiang, J. Wu, S. Poncin, H.Z. Li, Effect of hydrodynamic shear on biogas production and granule characteristics in a continuous stirred tank reactor, Process Biochem. 51 (2016) 345–351, https://doi.org/10.1016/j.procbio.2015.12.014.

[15] K. Takahashi, Mixing of pseduplastic liquid in a vessel equipped with a variety of helical ribbon impellers, J. Chem. Eng. Jpn. 45 (1979) 63–68.

[16] Y.Y. Tsui, Y.C. Hu, Flow characteristics in mixers agitated by helical ribbon blade impeller, Eng. Appl. Comput. Fluid Mech. 5 (2011) 416–429, https://doi.org/10.1080/19942060.2011.11015383.

[17] Y. Bao, Y. Lu, Q. Liang, L. Li, Z. Gao, X. Huang, S. Qin, Power demand and mixing performance of coaxial mixers in a stirred tank with CMC solution, Chinese J. Chem. Eng. 23 (2015) 623–632, https://doi.org/10.1016/j.cjche.2015.01.002.

[18] H. Ameur, M. Bouzit, Mixing in shear thinning fluids, Braz. J. Chem. Eng. 29 (2012) 349–358, https://doi.org/10.1590/S0104-66322012000200015.

[19] A. Delafosse, M.L. Collignon, S. Calvo, F. Delvigne, M. Crine, P. Thonart, D. Toye, CFD-based compartment model for description of mixing in bioreactors, Chem. Eng. Sci. 106 (2014) 76–85, https://doi.org/10.1016/j.ces.2013.11.033.

[20] P. Taylor, R.A. Ghotli, A.A.A. Raman, S. Ibrahim, LIQUID-LIQUID MIXING IN STIRRED VESSELS : A REVIEW Liquid-Liquid Mixing in Stirred Vessels : A Review, (n.d.) 37–41. doi:10.1080/00986445.2012.717313.

[21] B.S. Foucault, G. Ascanio, P.A. Tanguy, Coaxial Mixer Hydrodynamics With Newtonian and Non-newtonian Fluids, (2004), https://doi.org/10.1002/ceat.200401996.

[22] D.W.A.T.I. Hari-prajitno, P. Ved, T. Centre, B. Birmingham, Gas-Liquid Mixing Studies With Multiple up- and Down- Pumping Hydrofoil Impellers : Power Characteristics and Mixing Time, (1998), p. 76.

[23] Y. Kato, H. Furukawa, Y. Ikeda, T. Nakanishi, T. Sano, K. Tomioka, Development of a mixing process using an HB-type impeller to easily achieve scale-up by maintaining geometrical similarity, Int. J. Chem. Eng. 2018 (2018).

[24] Y. Bao, Y. Lu, Q. Liang, L. Li, Z. Gao, X. Huang, S. Qin, Power demand and mixing performance of coaxial mixers in a stirred tank with CMC solution Chinese Journal of Chemical Engineering Power demand and mixing performance of coaxial mixers in a stirred tank with CMC solution, Chin. J. Chem. Eng. (2018), https://doi.org/10.1016/j.cjche.2015.01.002.

[25] S. Deans, Techniques for Mixing and Scaling in Mechanically Agitated Vessels, (n.d.).

[26] T. Kouda, H. Yano, F. Yoshinaga, M. Kaminoyama, M. Kamiwano, Characterization of non-newtonian behavior during mixing of bacterial cellulose in a bioreactor, J. Ferment. Bioeng. 82 (1996) 382–386, https://doi.org/10.1016/0922-338X(96)89155-0.

[27] D. Hari-Prajitno, V.P. Mishra, K. Takenaka, W. Bujalski, A.W. Nienow, J. McKemmie, Gas-liquid mixing studies with multiple up- and down-pumping hydrofoil impellers: power characteristics and mixing time, Can. J. Chem. Eng. 76 (1998) 1056–1068, https://doi.org/10.1002/cjce.5450760612.

[28] K. Takahashi, N. Sugawara, Y. Takahata, Mixing time in an agitated vessel equipped with large impeller, J. Chem. Eng. Jpn. 48 (2015) 513–517, https://doi.org/10.1252/jcej.14we192.

[29] L. Lehrer, Mixing Time Prediction, Gas. 2, (1983), p. 2 http://www.mech.eng.unimelb.edu.au/people/staffresearch/AFMSsite/8/Lehrer2.pdf.

[30] M. Bouaifi, M. Roustan, Power consumption, mixing time and homogenisation energy in dual-impeller agitated gas-liquid reactors, Chem. Eng. Process. 40 (2001) 87–95, https://doi.org/10.1016/S0255-2701(00)00128-8.

[31] B.V. Machon, M. Jahoda, Liquid homogenization in aerated multi-impellers stirred vessel, Chem. Eng. Technol. 23 (2012), https://doi.org/10.1201/b11330-2 1–1.

[32] N. Hashemi, F. Ein-Mozaffari, S.R. Upreti, D.K. Hwang, Experimental investigation of the bubble behavior in an aerated coaxial mixing vessel through electrical resistance tomography (ERT), Chem. Eng. J. 289 (2016) 402–412, https://doi.org/10.1016/j.cej.2015.12.077.

[33] S.C. Low, D. Allitt, N. Eshtiaghi, R. Parthasarathy, Measuring active volume using electrical resistance tomography in a gas-sparged model anaerobic digester, Chem. Eng. Res. Des. 130 (2018) 42–51, https://doi.org/10.1016/j.cherd.2017.11.039.

[34] A. Einsele, R.K. Flnn, Influence of gas flow rates and gas holdup on blending efficiency in stirred tanks - industrial & engineering chemistry process design and development (ACS publications), Ind. Eng. Chem. (1980) 600–603.

[35] N. Blakebrough, K. Sambamurthy, Mass transfer and mixing rates in fermentation vessels, Biotechnol. Bioeng. 8 (1966) 25–42, https://doi.org/10.1002/bit.260080104.

[36] B.V. Machon, M. Jahoda, Liquid homogenization in aerated multi-impeller stirred vessel, Technol. Med. Sci. 23 (2012), https://doi.org/10.1201/b11330-2 1–1.
[37] N. Hashemi, F. Ein-Mozaffari, S.R. Upreti, D.K. Hwang, Analysis of mixing in an aerated reactor equipped with the coaxial mixer through electrical resistance tomography and response surface method, Chem. Eng. Res. Des. 109 (2016) 734–752, https://doi.org/10.1016/j.cherd.2016.03.028.
[38] J.C. Baudez, Physical aging and thixothropy in sludge rheology, Appl. Rheol. 18 (2007) 1–8.
[39] J.M. Smith, Dispersion of gases in liquids: the hydrodynamics of gas dispersion in low viscosity liquids, Mix. Liq. by Mech. Agit. (1985) 342.
[40] A. Paglianti, S. Pintus, M. Giona, Time-series analysis approach for the identification of flooding/loading transition in gas-liquid stirred tank reactors, Chem. Eng. Sci. 55 (2000) 5793–5802, https://doi.org/10.1016/S0009-2509(00)00125-1.
[41] R.P. Chhabra, L. Bouvier, G. Delaplace, G. Cuvelier, S. Domenek, C. André, Determination of mixing times with helical ribbon mipeller for non-Newtonian viscous fluids using an advanced imaging method, Chem. Eng. Technol. 30 (2007) 1686–1691, https://doi.org/10.1002/ceat.200700320.
[42] P. Ayazi Shamlou, M.F. Edwards, Power consumption of helical ribbon mixers in viscous newtonian and non-newtonian fluids, Chem. Eng. Sci. 40 (1985) 1773–1781, https://doi.org/10.1016/0009-2509(85)80040-3.
[43] F. Rieger, V. Novak, H. Dagmar, Homogenization efficiency of helical ribbon agitators, Chem. Eng. J. J. 33 (1986) 143–150, https://doi.org/10.1016/0300-9467(86)80013-2.
[44] H. Ameur, Y. Kamla, D. Sahel, Performance of helical ribbon and screw impellers for mixing viscous fluids in cylindrical reactors, Chemeng. J. 2 (2018) 1–9, https://doi.org/10.3390/chemengineering2020026.
[45] J. Cheng, P.I. Carreau, Aerated mixing of viscoelastic fluids with helical ribbon impellers, Chem. Eng. Sci. 49 (1994) 1965–1972.
[46] K. Takahashi, T. Yokota, H. Konno, Power consumption of helical ribbon agitators in highly viscous pseudoplastic liquids, J. Chem. Eng. Jpn. 17 (1984) 657–659, https://doi.org/10.1252/jcej.17.657.
[47] V.V. Chavan, J. Ulbrecht, Power correlations for close-clearance helical impellers in non-newtonian liquids, Ind. Eng. Chem. Process Des. Dev. 12 (1973) 472–476, https://doi.org/10.1021/i260048a015.
[48] E. Brito-De La Fuente, L. Choplin, P.A. Tanguy, Mixing with helical ribbon impellers: effect of highly shear thinning behaviour and impeller geometry, Chem. Eng. Res. Des. 75 (1997) 45–52, https://doi.org/10.1205/026387697523381.
[49] M. Amiraftabi, Khiadani Mehdi, Transparent polymers to emulate the rheological properties of primary, activated, and digested sludge authors, Chem. Eng. Res. Des. (2019), https://doi.org/10.1016/j.mex.2019.03.017.
[50] G. Delaplace, L. Bouvier, A. Moreau, R. Guérin, J.C. Leuliet, Determination of mixing time by colourimetric diagnosis - Application to a new mixing system, Exp. Fluids 36 (2004) 437–443, https://doi.org/10.1007/s00348-003-0741-7.
[51] F. Cabaret, S. Bonnot, L. Fradette, P.A. Tanguy, Mixing time analysis using colorimetric methods and image processing, Ind. Eng. Chem. Res. 46 (2007) 5032–5042, https://doi.org/10.1021/ie0613265.
[52] A.B. Metzner, R.E. Otto, Agitation of non-Newtonian fluids, AIChE J. 3 (1957) 3–10, https://doi.org/10.1002/aic.690030103.
[53] R. Baxter, N. Hastings, A. Law, E.J. Glass, Food Stabilisers, Thickeners and Gelling Agent, (2008).
[54] S. Nagata, M. Nishikawa, T. Hisayuki, H. Hirabayashi, S. Gotoh, Power consumption of mixing impellers Bingham plastic liquids, J. Chem. Eng. Jpn. 3 (1970) 237–243, https://doi.org/10.1252/jcej.3.237.
[55] M. Houska, Anchor-agitated systems : power input correlation for pseudoplastic and thixotropic fluids in equilibrium, AIChE J. 32 (1986) 155–158, https://doi.org/10.1002/aic.690320119.
[56] J. Cheng, P.J. Carreau, Aerated mixing of viscoelastic fluids with helical ribbons impellers, Chem. Eng. Sci. 49 (1994) 1965–1972, https://doi.org/10.1016/0009-2509(94)80080-4.
[57] M. Moo-Young, K. Tichar, F.A.L. Dullien, The blending efficiencies of some impellers in batch mixing, AIChE J. 18 (1972) 178–182, https://doi.org/10.1002/aic.690180133.
[58] H. Ameur, Energy efficiency of different impellers in stirred tank reactors, Energy 93 (2015) 1980–1988, https://doi.org/10.1016/j.energy.2015.10.084.
[59] J. Wu, Y. Zhu, L. Pullum, The effect of impeller pumping and fluid, Can. J. Chem. Eng. 79 (2001) 177–186, https://doi.org/10.1002/cjce.5450790201.
[60] E.L. Paul, V. a Atiemo-obeng, S.M. Kresta, Handbook of Inductrial Mixing, (2004), https://doi.org/10.1002/0471451452.
[61] J. Wu, H. ming Zhou, H. zhi Li, P. cheng Zhang, J. Jiang, Impacts of hydrodynamic shear force on nucleation of flocculent sludge in anaerobic reactor, Water Res. 43 (2009) 3029–3036, https://doi.org/10.1016/j.watres.2009.04.026.
[62] M. hui Xie, J. ye Xia, Z. Zhou, G. zhong Zhou, J. Chu, Y. ping Zhuang, S. liang Zhang, H. Noorman, Power consumption, local and average volumetric mass transfer coefficient in multiple-impeller stirred bioreactors for xanthan gum solutions, Chem. Eng. Sci. 106 (2014) 144–156, https://doi.org/10.1016/j.ces.2013.10.032.
[63] H. Bourne, J.R. Buttler, Power consumption of helical ribbon impellers in viscose liquids, Process Saf. Environ. Prot. 47 (1969).
[64] V.C. Zitrom, One-factor-at-a-time versus designed experiments, Am. Stat. 53 (1999) 126–131, https://doi.org/10.2307/2685731.
[65] L. Wiedemann, F. Conti, T. Janus, M. Sonnleitner, W. Zörner, M. Goldbrunner, Mixing in biogas digesters and development of an artificial substrate for laboratory-scale mixing optimization, Chem. Eng. Technol. 40 (2017) 238–247, https://doi.org/10.1002/ceat.201600194.
[66] X.H. Yang, W.L. Zhu, Viscosity properties of sodium carboxymethylcellulose solutions, Cellulose 14 (2007) 409–417, https://doi.org/10.1007/s10570-007-9137-9.
[67] D. Patel, F. Ein-Mozaffari, M. Mehrvar, Improving the dynamic performance of continuous-flow mixing of pseudoplastic fluids possessing yield stress using Maxblend impeller, Chem. Eng. Res. Des. 90 (2012) 514–523, https://doi.org/10.1016/j.cherd.2011.08.022.
[68] M. Fujasová, V. Linek, T. Moucha, E. Prokopová, Energy demands of different impeller types in gas – liquid dispersions, Sep. Purif. Technol. 39 (2004) 123–131, https://doi.org/10.1016/j.seppur.2003.12.015.
[69] D. Patel, F. Ein-Mozaffari, M. Mehrvar, Improving the dynamic performance of continuous-flow mixing of pseudoplastic fluids possessing yield stress using Maxblend impeller, Chem. Eng. Res. Des. 90 (2012) 514–523, https://doi.org/10.1016/j.cherd.2011.08.022.
[70] A. Bombač, M. Žumer, I. Žun, Power consumption in mixing and aerating of shear thinning fluid in a stirred vessel, Chem. Biochem. Eng. Q. 21 (2007) 131–138.
[71] S.L.C. Ferreira, R.E. Bruns, H.S. Ferreira, G.D. Matos, J.M. David, G.C. Brandão, E.G.P. da Silva, L.A. Portugal, P.S. dos Reis, A.S. Souza, W.N.L. dos Santos, Box-Behnken design: an alternative for the optimization of analytical methods, Anal. Chim. Acta 597 (2007) 179–186, https://doi.org/10.1016/j.aca.2007.07.011.